Hydrocarbon injection for quantification of chemical erosion yields in tokamaks

S.Brezinsek[a*], A.Pospieszczyk[a], D.Borodin[a], M.F.Stamp[b], R.Pugno[c], A.G.McLean[d], U.Fantz[c], A.Manhard[c], A.Kallenbach[c], N.H.Brooks[e], M.Groth[f], Ph.Mertens[a], V.Philipps[a], U.Samm[a] and TEXTOR, ASDEX Upgrade, DIII-D teams and JET-EFDA contributors[⋆]

[a] *Institut für Plasmaphysik, Forschungszentrum Jülich, Association EURATOM-FZJ, Trilateral Euregio Cluster, Germany, www.fz-juelich.de/ipp*

[b] *Euratom/UKAEA Fusion Association, Culham Science Centre, Abingdon, Oxon OX14 3DB, UK*

[c] *Max-Planck-Institut für Plasmaphysik, IPP-EURATOM Association, " D-85748 Garching, Germany*

[d] *University of Toronto, Department of Aerospace Studies, Canada*

[e] *General Atomics, San-Diego, CA, USA*

[f] *Lawrence Livermore National Laboratory, Livermore, USA*

[⋆] *See annex of J. Pamela et al., Fusion Energy 2002 (19th Int. Conf., Lyon, 2002), IAEA, Vienna*

Abstract

Chemical erosion of carbon can be described as function of the incident ion flux, the ion energy and the surface temperature. Spectroscopy on the hydrocarbon break-up products CH and C_2 is applied to determine in-situ hydrocarbon fluxes and quantify the chemical erosion by means of hydrocarbon injection. Present-day knowledge on critical issues concerning the erosion yield and its determination is presented: Effective inverse photon efficiencies are measured in TEXTOR for different hydrocarbon species and compared with calculations from HYDKIN. The underlying database for the methane break-up, used in different erosion/deposition models, has been put to test. The chemical erosion yield related to higher hydrocarbons is determined to be lower in the JET outer divertor than measured in previous experiments. In ASDEX Upgrade and DIII-D first in-situ calibrations of hydrocarbon fluxes in the detached outer divertor are performed.

PACS: 52.70.Kz, 52.40.Hf, 52.25.Vy, 52.55.Fa, 33.20.Lg

JNM keywords: Carbon, Impurities, Plasma-Materials Interaction, Redeposition, Surface effects

PSI-16 keywords: Spectroscopy, ITER, Carbon impurities, Erosion & Deposition, Divertor

Corresponding author address: Institut für Plasmaphysik, Forschungszentrum Jülich GmbH, D-52425 Jülich, Germany

Corresponding author e-mail: s.brezinsek@fz-juelich.de

Presenting author: Sebastijan Brezinsek

Presenting author e-mail: s.brezinsek@fz-juelich.de

1. Introduction

The use of carbon-based materials for plasma-facing components (pfc) in fusion devices is connected to the appearance of chemical erosion, followed by carbon migration and deposition. The main chamber has been identified as one of the main sources of eroded carbon, and marker experiments indicated a stepwise transport of carbon towards the deposition-dominated inner divertor [1]. The outer divertor often exhibits balanced erosion/deposition, though net erosion has been observed in some devices [2]. The experimental determination of carbon fluxes -atomic and molecular ones- is crucial for the understanding of migration and verification of erosion/deposition codes [3] which are used for predictions of erosion and tritium co-deposition in the ITER divertor.

Passive emission spectroscopy has access to fluxes Γ_C of carbon in different ionisation states as well as of molecular fragments of hydrocarbons, in particular CH and C_2 radicals, and thus, to the physical sputtering Y_C^{phys} and chemical erosion yield Y_C^{chem}. Y_C^{chem} can be described as a function of ion energy, ion flux and surface temperature [4], though uncertainties with respect, among others, to data interpretation, higher hydrocarbons and extrapolation to detached plasma regimes exist.

Essential for the Y_C^{chem} is the quantification of Γ_C^{chem} which is made with the aid of photon fluxes ϕ of hydrocarbon break-up products and effective inverse photon efficiencies. This indirect conversion includes the dissociation chain and has been identified as a critical issue. In-situ calibration with injection of hydrocarbons takes into account local conditions like plasma parameters, surface properties and geometry.

2. The spectroscopic approach to determine Γ_C^{chem} and Y_C^{chem}

Spectroscopy is used to determine particle fluxes in fusion devices [5]. Photon fluxes are converted into particle fluxes with the aid of inverse photon efficiencies, or so-called S/XB or D/XB values. There S stands for the ionisation rate coefficient of an atom, D for the

decay rate coefficient of a molecule which represents its "loss" by either dissociation or ionisation, and XB is the excitation rate coefficient of the observed transition weighted with the branching ratio for a given set of electron density n_e and temperature T_e.

The carbon flux $\Gamma_C^{total} = \Gamma_C^{chem} + \Gamma_C^{phys}$ can be deduced by observation of carbon ion radiation, i.e. CII, and due consideration of corresponding S/XB values from ADAS [6]. Although this emission is localised in the plasma edge, no information about the source processes, whether involving physical or chemical sputtering, can be obtained. The hydrocarbon flux Γ_C^{chem} and with it $Y_C^{chem} \simeq \frac{\Gamma_C^{chem}}{\Gamma_D}$, the flux ratio of chemically eroded carbon to the impinging hydrogen, is needed to distinguish between these processes. The recycling flux Γ_D [7] is assumed to be equivalent to the impinging ion flux.

2.1 Photon fluxes and effective inverse photon efficiencies for hydrocarbons

The carbon flux Γ_C^{chem} originates from molecules of the methane (CH_x with $x \leq 4$), the ethane (C_2H_y with $y \leq 6$) and the propane family (C_3H_z with $z \leq 8$) and is given by $\Gamma_C^{chem} = \Gamma_C^{CH_x} + 2\Gamma_C^{C_2H_y} + 3\Gamma_C^{C_3H_z} + ...$ The initial hydrocarbon as well as the main part of molecular ions or radicals built up along the complex destruction path [8] in the plasma cannot be detected by emission spectroscopy. Only CH , CH^+ and C_2 can be observed; the CH Gerö band, main representative for CH_x, the C_2 Swan band, representative for C_2H_y, and the CH^+ Douglas-Herzberg band are the main recorded transitions in fusion-related plasmas [9]. Effective D/XB values include the dissociation chain for given plasma parameters [10]. For CH_x and C_2H_y the important ones are:

$$\left[\frac{D}{XB}\right]^{C_2H_y \rightarrow C_2}_{\mathrm{d}\ ^3\Pi \rightarrow \mathrm{a}\ ^3\Pi} = \frac{\Gamma^{C_2H_y}}{\phi^{C_2H_y \rightarrow C_2}_{\mathrm{d}\ ^3\Pi \rightarrow \mathrm{a}\ ^3\Pi}} \text{ and } \left[\frac{D}{XB}\right]^{CH_x \rightarrow CH}_{\mathrm{A}\ ^2\Delta \rightarrow \mathrm{X}\ ^2\Pi} = \frac{\Gamma^{CH_x}}{\phi^{CH_x \rightarrow CH}_{\mathrm{A}\ ^2\Delta \rightarrow \mathrm{X}\ ^2\Pi}} \left[\frac{D}{XB}\right]^{C_2H_y \rightarrow CH}_{\mathrm{A}\ ^2\Delta \rightarrow \mathrm{X}\ ^2\Pi} = \frac{\Gamma^{C_2H_y}}{\phi^{C_2H_y \rightarrow CH}_{\mathrm{A}\ ^2\Delta \rightarrow \mathrm{X}\ ^2\Pi}}$$

Fig.1a shows examples of spectra and simulations for the Douglas-Herzberg and the Gerö bands. Reduced spectral ranges are chosen to cover a contamination-free representative portion of the band. Different wavelength ranges (λ_{span}) for the CD Gerö band are in use:

429.5-431.0nm at TEXTOR [10], ASDEX Upgrade [11] and JT-60U [12], which cover the first 1.5nm at the band head, as well as 427.0-431.5nm at DIII-D [13] and 427.8-431.5nm at JET [14].Data for the CH and CD Gerö band presented here are normalised to the full spectral range of the electronic transition (spanning: 415.0-445.0nm) by multiplying with calculated expansion factors $f_{A-X}^{CH\ or\ CD}(T_{rot}, \lambda_{span})$ [10,11] except where other indications are made. These expansion factors are determined by the ratio of the light emission in λ_{span} to the total light emission of the A-X band which can be obtained from spectra fitting or simulation for a given ro-vibrational population [15]. Data for the C_2 Swan band are normalised in a similar way with the aid of $f_{d-a}^{C_2}(T_{rot}, \lambda_{span})$ (see sec.3).

2.2 Experimental realisation of injection experiments

Calibration experiments with injection of stable hydrocarbons are carried out to determine effective D/XB values and, thus, to relate the emitted photon flux of hydrocarbon fragments to the flux of injected hydrocarbon particles. The individual injection rate is chosen high enough to ensure significant photon fluxes from the injection with respect to the intrinsic background and low enough to minimise plasma disturbances. Apart from JET, where a multiple injection through toroidally circumferential gas inlets is made [14], all other experiments presented here are done with single injections.

In the case of circumferential injection at JET ($\sim 2 \cdot 10^{21} \frac{part.}{s}$), a toroidally homogeneous distribution of the injected gas in the observation volume is assumed. The edge plasma is disturbed and reference discharges are necessary to take changes in the hydrocarbon source strength into account. Experimentally determined quantities are averages over large areas. Note that recent experiments in DIII-D with circumferential injection of methane through the upper plenum were performed without significant disturbance of the edge plasma parameters [16].

In the case of single gas injections ($0.5 - 15 \cdot 10^{18} \frac{part.}{s}$), a perturbation of the local plasma

parameters at a representative location occurs but reference discharges are unnecessary due to the low degree of perturbation. The observation volume has to be chosen large enough to ensure that all photons induced by the gas injection are detected. Transfer to other locations might be affected by uncertainties [17]. At ASDEX Upgrade [18] and DIII-D [19] the gas injection systems, discussed here, are integral part of the outer divertor and thus embedded in carbon-based target plates. The porous-plug injector PPI is in particular in use to simulate the chemically eroded carbon by injection through micro holes. At TEXTOR, different injection systems, either integrated in limiters or in metallic tubes, have been applied in a flexible vacuum lock system [7].

3. Experimentally determined and calculated effective inverse photon efficiencies

Spectrum simulations of the Gerö and the Swan band in different experiments have shown that the ro-vibrational populations, and therewith the expansion factors, are quite robust and vary only slightly with plasma parameters. Typical rotational temperatures have been found for a wide range of plasma parameters: 3500+/-500 K for the Gerö band with $f^{CD}_{A-X}(T_{rot} = 3500K, \lambda_{span} = 429.5nm - 431.0nm) = 2.8$ and $f^{CH}_{A-X}(T_{rot} = 3500K, \lambda_{span} = 430.0nm - 431.5nm) = 2.8$ for the complete $A - X$ transition and 3000+/-1000 K for the Swan band with $f^{C_2}_{d-a}(T_{rot} = 3000K, \lambda_{span} = 515.3nm - 516.6nm) = 4$ for the main diagonals ($\Delta v = 0$ with $v = 0 - 3$) of the $d - a$ transition. The origin of the C_2 molecule seems to plays no role, even sublimated C_2, observed at an accidently overheated graphite protection tile in TEXTOR, shows for comparable plasma conditions an almost identical ro-vibrational population in comparison to C_2 from hydrocarbon injections (fig.1b).

3.1 Effective D/XB values for different hydrocarbons in TEXTOR

A benchmark experiment in TEXTOR has been performed to validate the underlying data base for the hydrocarbon break-up [8] used in the ERO code. Different hydrocarbons were injected in D or H plasmas. The use of different isotopes allows to distinguish between CD

and CH as well as between D and H from the break-up and the plasma background. The observation volume was chosen large enough to ensure that molecular hydrocarbon fragments of type CH or C_2 are either dissociated or ionised before leaving the observation volume. Losses due to transport out of the volume can be excluded. 2D images from top and from the side recorded with intensified CCD cameras equipped with interference filters for the observed transitions were used for verification (fig.2a). Gas inlet and observation volume were free of graphite surfaces, thus no intrinsic neutral and molecular carbon was detectable prior to the injection. Moreover, no significant surface area for local deposition exists within the observation volume under consideration of the short penetration depth of the fragments (fig.2b). The observed light emission can be referred completely to the bare impact of the plasma on the injected hydrocarbons; secondary effects caused by either sinks or sources of hydrocarbons at surfaces can be excluded.

D/XB values for the different injected species (tab.1) were related to the edge plasma parameters at the position of maximum light emission (fig.2b). These are in the case of D plasmas: $n_e = 2.2 \cdot 10^{18} m^{-3}$ and $T_e = 35eV$ and in the case of H plasmas: $n_e = 1.8 \cdot 10^{18} m^{-3}$ and $T_e = 45eV$ as taken from the outer midplane and measured by Langmuir probes [20] or He-beam diagnostics [21]. These non-local edge plasma parameters were not influenced by the hydrocarbon injection. Local measurement of T_e by a Langmuir probe, installed for comparable experiments directly next to the gas inlet, indicate a slight reduction of T_e of less than 15% during the injection. This grade of disturbance is in-line with T_e measurements during the hydrocarbon injection obtained from the analysis of the Balmer-β to Balmer-γ line ratio in the emission cloud of the background plasma. The gas inlet was positioned 1.5cm (H) and 2.0cm (D) behind the LCFS. The uncertainty in each effective D/XB values is below 20%.

D/XB values for CH and CD denoted with JR are calculated with the aid of HYDKIN [22],

a reaction kinetic analysis solver for the catabolism of hydrocarbon in hydrogen plasmas, and vibrationally resolved emission rate coefficients for the Gerö band. These vibrationally resolved emission rate coefficients are 1.48 times larger than the non-vibrational resolved ones [11] which are ordinary applied in HYDKIN (memo in [22]). The effective D/XB values presented here are diminished by this factor 1.48 in comparison with the standard HYDKIN output.

HYDKIN assumes a constant plasma background as input parameter. The calculation of D/XB values is reasonable as long as the variation of the involved rate coefficients is small in the plasma parameter range where the molecular fragments exist. The ERO code [3] takes additionally the transport, the edge plasma parameters profiles and the local geometry into account. Modelling has so far only been applied for CD_4 (fig.2c). $\left[\frac{D}{XB}\right]^{CD_4 \rightarrow CD}_{\mathrm{A}\ ^2\Delta \rightarrow \mathrm{X}\ ^2\Pi}$ from ERO amounts to 32 and is in agreement with the experimental value of 36, and slightly lower than the HYDKIN value of 46. Thus, the database for the methane break-up [8] is reliable in the plasma parameter range of TEXTOR. However, ERO modelling is needed for an exact interpretation of the injection experiments, but HYDKIN calculations can be applied as a step in testing the database.

Photon efficiencies for C_2 and CH from C_2H_y and C_3H_z calculated with HYDKIN and the emission rate coefficient for the Swan band [11] are comparable with the measured values, they differ at most by a factor of 2, where less CH light and more C_2 light is predicted from calculations. This indicates uncertainties in the database for C_2H_y and C_3H_z with respect to the branching ratio of higher hydrocarbons.

Information about the break-up reactions can be deduced from effective inverse photon efficiencies for C, C^+, and H, build along the dissociation chain. These conversion factors, normalised to the number of C atoms or H atoms in the initial hydrocarbon, can be related to bare S/XB values from ADAS for atoms and ions. The ratio $\left[\frac{S}{XB}\right]_{ADAS} / \left[\frac{D}{XB}\right]_{EXP}$ for

the different fragments and their electronic transitions is defined as the normalised photon-per-particle production efficiency η. For CH_4 the following values $\left[\frac{D}{XB}\right]^{CH_4 \rightarrow C}_{\text{CI 909.5nm}} = 72$ with $\eta = 0.20$, $\left[\frac{D}{XB}\right]^{CH_4 \rightarrow C^+}_{\text{CII 426.7nm}} = 277$ with $\eta = 0.56$, $\left[\frac{D}{XB}\right]^{CH_4 \rightarrow H}_{\text{H}_\gamma} = 390$ with $\eta = 0.19$ were determined.

$\eta < 1$ means that less photons per particle are observed during the break-up than expected from the bare number of C or H particles in the initial hydrocarbon. For example, the number of $CI(909.5nm)$ photons emitted per CH_4 launched into the plasma is only 20% of the number that would be calculated using ADAS per isolated C atom launched into the same plasma. Either less photons are emitted, e.g. due to dissociation of a molecular fragment into an atom or ion which is directly excited in a higher electronic state than the upper state of the observed transition, or more likely, less fragments of the observed kind are produced during the catabolism, e.g. absence of neutral C due to dissociation of CD^+ into D and C^+. In the case of hydrogen: the absence of a large fraction of photons per atom ($\eta \simeq 0.2$) has been observed transition-independently for H_β, H_γ, and H_δ. Only about 20% of the expected hydrogen atoms have been detected, thus probably more protons than atoms are built up during the break-up. In the case of the carbon balance: on the one hand only 20% of the theoretically possible $CI(909.5nm)$ photons per neutral C are detected, and on the other hand the number of $CII(426.7nm)$ photons per C^+ is about a half that theoretically possible. However, more CI and CII transitions have to be analysed to discriminate the two possible effects mentioned above, the large difference in the efficiency for C and C^+ indicates that the destruction path, though it is a multi-step process, goes substantially via molecular ions, which is in-line with HYDKIN calculations and the prominent presence of the CD^+ A-X band (fig.1a) in TEXTOR.

3.2 Effective D/XB values for methane from different devices

A set of data from different experiments exists for ohmic or L-mode discharges with injec-

tion of CH_4/CD_4 into outer divertor plasmas. At JET the injection was into the private flux region PFR. $\left[\frac{D}{XB}\right]^{CH_4\rightarrow CH}_{\mathrm{A}\ ^2\Delta\rightarrow\mathrm{X}\ ^2\Pi}$ related to the full band emission was determined to 55-60 [10,23] when the outer-strike point was on the vertical target ($T_e = 40eV,\ n_e = 6\cdot 10^{19}m^{-3}$). Though the toroidally homogeneity of the injection cloud is given in vertical configuration, a minor loss of particles into the inner divertor and to the pump duct of the outer divertor cannot be excluded and $\left[\frac{D}{XB}\right]^{CH_4\rightarrow CH}_{\mathrm{A}\ ^2\Delta\rightarrow\mathrm{X}\ ^2\Pi} = 55$ is an upper limit. Similar values, but for lower T_e were reported in previous experiments [14].

At DIII-D the injection was into the scrape-off layer (SOL) ($T_e = 22.5eV,\ n_e = 2.5\cdot 10^{19}m^{-3}$) and $\left[\frac{D}{XB}\right]^{CH_4\rightarrow CH}_{\mathrm{A}\ ^2\Delta\rightarrow\mathrm{X}\ ^2\Pi}$ was determined to 40+/-11 [19] when normalised to the full band. At ASDEX Upgrade methane injection into the PFR and SOL for high density hydrogen plasmas is well described [24]. The D/XB value related to the Gerö band varies between 4 and 20 for $n_e = 2...8\cdot 10^{19}m^{-3}$ and $T_e = 5...15eV$).

Fig.3 shows an overview of $\left[\frac{D}{XB}\right]^{CH_4\rightarrow CH}_{\mathrm{A}\ ^2\Delta\rightarrow\mathrm{X}\ ^2\Pi}$ and $\left[\frac{D}{XB}\right]^{CD_4\rightarrow CD}_{\mathrm{A}\ ^2\Delta\rightarrow\mathrm{X}\ ^2\Pi}$ from the different experiments compared with calculated values (HYDKIN) as function of T_e. Additional experimental data, in particular from TEXTOR, was added and, for clarification, in some cases only representative points were taken from a larger set of data. The corresponding λ_{span} and $f(T_{rot}, \lambda_{span})$ values which were applied for the normalisation are given in tab.2.

Though different local conditions and geometries are involved, the general increase of $\left[\frac{D}{XB}\right]^{CH_4\rightarrow CH}_{\mathrm{A}\ ^2\Delta\rightarrow\mathrm{X}\ ^2\Pi}$ with T_e, as calculated with HYDKIN, is well reproduced, indicating both the reliability of the underlying database for the methane break-up chain and the general consistency of experimental results over a wide plasma parameter range. However, in detail the experimental data with graphite surrounding shows higher effective D/XB values, which means less light is observed than expected from HYDKIN. This discrepancy might be attributed to the simplified assumption of a constant plasma, to a loss of particles during the injection due to deposition or transport, or to changes in local conditions. For a more

detailed comparison ERO calculations for each experiment are needed which are here out of the scope.

3.3 Injection-induced re-erosion of higher hydrocarbons

The experimentally determined $\left[\frac{D}{XB}\right]^{CH_4 \rightarrow CH}_{\mathrm{A}\ ^2\Delta \rightarrow \mathrm{X}\ ^2\Pi}$ shows no indication of enhancement due to an additional source in the presence of a graphite surrounding. However, experiments with CH_4 injection show an accompanying emission of C_2 light when the injection was through gas inlets surrounded by graphite or when graphite layers are present.

In fig.4 the time evolution of $\phi^{C_2}_{d-a}$ during methane injection ($3 \cdot 10^{18} \frac{part.}{s}$) in the attached outer divertor of ASDEX Upgrade is shown. The outer strike point was swept twice over the local injection. Low intrinsic $\phi^{C_2}_{d-a}$ was detected in the reference phase, whereas with CH_4 injection a strong and nearly instantaneous increase of $\phi^{C_2}_{d-a}$ up to a factor six was observed. The present understanding is: a fraction of the injected methane is locally deposited and immediately, with a high erosion rate re-eroded, substantially as higher hydrocarbon. In the consecutive discharge, apart from an increased emission during the strike-point formation no enhanced emission of C_2 light was observed. These observations are similar to experiments with the PPI [19], where also an increase of $\phi^{C_2}_{d-a}$ with methane injection was measured. The C_2 light decreased in the subsequent discharges without injection. This dynamic process as well as the contribution of possible re-eroded methane to the CH light emission is a topic of present modelling with erosion deposition codes.

4. Hydrocarbon fluxes and erosion yields

Because of the limited space I confine myself on three examples, one which deals with the contribution of ethene to Y^{chem}_C, one which indicates the improved understanding of data analysis, and one which investigates the hydrocarbon flux in detached divertor plasmas.

4.1. The contribution of C_2H_y to Y^{chem}_C in the JET outer divertor

In JET, calibration experiments were made in deuterium discharges (L-mode, $T_e = 25eV$

and $n_e = 5.5 \cdot 10^{19} m^{-3}$) with circumferential puffing of ethene through an injection module (GIM10) located between the vertical plates of the outer divertor. The outer strike point was swept over the injection locations, thus C_2H_4 was either injected in the near, the far SOL or in PFR [25]. A reference discharges with hydrogen injection was performed to match the plasma parameters. The injection through GIM10 into the scrape-off layer suffer from a gas bypass ($\sim$ 25% loss), the non-homogeneity of the injection ($\leq$ 40% of the expected gas reaches the observation volume) as well as from the cross-divertor transport ($\sim$ 10% loss) when the outer strike point is positioned near to the injection location. This has been recently identified in tracer injection experiments with the outer-strike point portioned slightly below GIM10 by the analysis of the local deposited ^{13}C [26]. Analysis and simulations are ongoing to determine the exact portion of injected gas reaching the observation volume described in [14].

However, an upper limit for the effective inverse photon efficiency $\left[\frac{D}{XB}\right]^{C_2H_4 \rightarrow C_2}_{\mathrm{d}\ ^3\Pi \rightarrow \mathrm{a}\ ^3\Pi}$ for the C_2 Swan band ($f^{C_2}_{d-a}(T_{rot} = 3000K, \lambda_{span} = 515.3nm - 516.6nm) = 4$) is determined to be below 75. Fig.5 shows the erosion yield distribution with the strike-point fixed on the poloidal location of GIM10. The erosion yield $Y_C^{chem,\ C_2H_y}$ is below 0.6% at the location with maximum impinging ion flux of about $1.65 \cdot 10^{23} \frac{ions}{s}$ at a surface temperature of about 450K. This is essentially less than reported in [14] where the injection was in the PFR. However, it is still above the predictions for the erosion yield from [3-4] which is for these conditions about 0.3%.

4.2. The total sputtering yield in TEXTOR

In TEXTOR a pre-heatable spherical graphite limiter was used to determine the erosion yield as function of the graphite temperature. The limiter was positioned at the LCFS ($n_e = 5.2 \cdot 10^{18} m^{-3}, T_e = 42eV, T_i = 150eV, \Gamma_{D^+} = 7.5 \cdot 10^{22}\ ions\ s^{-1} m^{-2}$) and pre-heated to 520 K before exposed to the plasma. Details on the applied spectroscopic systems and the

experimental conditions can be found in [7].

Fig. 6a shows the behaviour of CD and D_γ intensity, with variation of the bulk temperature under otherwise constant plasma parameters. Clearly, the decrease of CD intensity with higher surface temperatures and its complete absence at 1300K can be observed [27]. Also indicated is the behaviour of deuterium molecules, which disturbed the $A-X$ band and which were taken into account in the analysis [7]. However, above 1100K an increase of the D_γ intensity can also be observed. Deuterium starts to be directly released as atoms and not as molecules from the surface. The deuterium recycling flux can be obtained from the extrapolated D_γ maximum value, where the release is pure atomic [7]. The intensity ratio of D_γ from the maximum value to CD, multiplied with the ratio of the S/XB value for D_γ taken from ADAS to $\left[\frac{D}{XB}\right]^{CD_4\rightarrow CD}_{\mathrm{A}\ ^2\Delta\rightarrow\mathrm{X}\ ^2\Pi}$ deduced from injection experiments described before, provides Y_C^{chem}. Due to this correction the erosion yield is reduced from about $Y_C^{chem}=4.0\%$ to $Y_C^{chem}=3.0\%$ in comparison to [27].

Fig.6b shows Y_C^{total} deduced from the light intensity of CII at 426.7nm. The difference at highest temperatures, where Y_C^{chem} vanishes, represents Y_C^{phys}. In the case of TEXTOR Y_C^{chem} and Y_C^{phys} are almost balanced at the temperature of maximum erosion.

Although the yield determination is based only on the CD photon flux, contributions from other hydrocarbons than CD_4 are implicitly included: $\phi^{CD}_{\mathrm{A}\ ^2\Delta\rightarrow\mathrm{X}\ ^2\Pi}=\phi^{CD_x\rightarrow CD}_{\mathrm{A}\ ^2\Delta\rightarrow\mathrm{X}\ ^2\Pi}+\phi^{C_2D_y\rightarrow CD}_{\mathrm{A}\ ^2\Delta\rightarrow\mathrm{X}\ ^2\Pi}+....$ Conversion using $\left[\frac{D}{XB}\right]^{CD_x\rightarrow CD}_{\mathrm{A}\ ^2\Delta\rightarrow\mathrm{X}\ ^2\Pi}$ leads to the apparent particle flux $\tilde{\Gamma}_C^{CD_x}$ which overestimates $\Gamma_C^{CD_x}$ by the contribution of $\Gamma_C^{C_2D_y}$ to the CD photon flux.

Γ_C^{chem} can be described as function of the measured CD and C_2 photon fluxes:

$$\Gamma_C^{chem}=\tilde{\Gamma}_C^{CD_x}+(2-\frac{\left[\frac{D}{XB}\right]^{CD_x\rightarrow CD}_{\mathrm{A}\ ^2\Delta\rightarrow\mathrm{X}\ ^2\Pi}}{\left[\frac{D}{XB}\right]^{C_2D_y\rightarrow CH}_{\mathrm{A}\ ^2\Delta\rightarrow\mathrm{X}\ ^2\Pi}})\Gamma_C^{C_2D_y}=\tilde{\Gamma}_C^{CD_x}[1+\frac{\phi^{C_2}_{\mathrm{d}\ ^3\Pi\rightarrow\mathrm{a}\ ^3\Pi}}{\phi^{CD}_{\mathrm{A}\ ^2\Delta\rightarrow\mathrm{X}\ ^2\Pi}}\beta]$$

The correction of the apparent particle flux depends on $\phi^{C_2}_{\mathrm{d}\ ^3\Pi\rightarrow\mathrm{a}\ ^3\Pi}/\phi^{CD}_{\mathrm{A}\ ^2\Delta\rightarrow\mathrm{X}\ ^2\Pi}$ and on the branching ratio $\beta=2\frac{\left[\frac{D}{XB}\right]^{C_2D_y\rightarrow C_2}_{\mathrm{d}\ ^3\Pi\rightarrow\mathrm{a}\ ^3\Pi}}{\left[\frac{D}{XB}\right]^{CD_x\rightarrow CD}_{\mathrm{A}\ ^2\Delta\rightarrow\mathrm{X}\ ^2\Pi}}-\frac{\left[\frac{D}{XB}\right]^{C_2D_y\rightarrow C_2}_{\mathrm{d}\ ^3\Pi\rightarrow\mathrm{a}\ ^3\Pi}}{\left[\frac{D}{XB}\right]^{C_2D_y\rightarrow CH}_{\mathrm{A}\ ^2\Delta\rightarrow\mathrm{X}\ ^2\Pi}}$. Here, the correction for the erosion yield deduced from CD emission is about 1.1, whereas $\phi^{C_2}_{\mathrm{d}\ ^3\Pi\rightarrow\mathrm{a}\ ^3\Pi}\simeq 0.1\phi^{CD}_{\mathrm{A}\ ^2\Delta\rightarrow\mathrm{X}\ ^2\Pi}$ and

$\beta \simeq 1$. Thus, the measured CD light underestimates the total erosion yield by about 10%. Note that we have omitted in this approach an essential production of carbon dimers out of two methane break-up products as well as contributions from C_3D_z. In the case of the attached ASDEX Upgrade divertor in L-mode ($T_e \simeq 5 - 20eV$), the correction term is of the order of 1.3, whereas β is about 1 and $\phi^{C_2}_{\mathrm{d}\ ^3\Pi\rightarrow \mathrm{a}\ ^3\Pi}/\phi^{CD}_{\mathrm{A}\ ^2\Delta\rightarrow \mathrm{X}\ ^2\Pi} \simeq 0.3$ [11].

4.3 Hydrocarbon flux in detached plasmas

The operational regime for the outer divertor in ITER is a detached plasma. Not much information about the chemical erosion, the hydrocarbon fluxes and the effective inverse photon efficiencies for this regime is available yet. Previous experiments in DIII-D [28] have shown a reduction of the light emission of the C_2 Swan band and of the CH Gerö band when the outer divertor detaches under L-mode conditions. The reduction was attributed to the reduction of Γ_C^{chem} and Y_C^{chem}, though the effective D/XB values for CH_x and C_2H_y in detached plasma conditions were uncertain. Previous modelling predictions [28 and references therein] indicated for methane $\left[\frac{D}{XB}\right]^{CH_4\rightarrow CH}_{\mathrm{A}\ ^2\Delta\rightarrow \mathrm{X}\ ^2\Pi} = 5$, which is comparable with HYDKIN calculations for $T \simeq 1eV,\ n_e \simeq 2 \cdot 10^{20} m^{-3}$.

In ASDEX Upgrade, experiments in L-mode with detachment of the outer divertor by means of strong deuterium puffing were performed. Two sweeps of the outer strike-point over the gas injection location were made. Whilst the first one is used as reference, the second one is for the in-situ calibration of the photon fluxes with by CH_4 and C_2H_4 injection. In detachment a strong reduction of both the intrinsic photon flux of ϕ^{CD}_{A-X} (fig.7) and $\phi^{C_2}_{d-a}$ of more than a factor 12 was observed in comparison to an attached plasma reference. In the case of the CD A-X transition in detachment, strong disturbance (up to 50%) by the BD A-X transition was found and taken into consideration in the analysis.

With injection of either CH_4 or C_2H_4, a clear increase in the light emission was observed. The corresponding effective inverse photon efficiencies were determined to $\left[\frac{D}{XB}\right]^{CH_4\rightarrow CH}_{\mathrm{A}\ ^2\Delta\rightarrow \mathrm{X}\ ^2\Pi} =$

$18 +/- 7$ and $\left[\frac{D}{XB}\right]^{C_2H_y \rightarrow CH}_{\mathrm{A}\ ^2\Delta \rightarrow \mathrm{X}\ ^2\Pi} = 47 +/- 19$. The value for methane is about 1.2-4.0 times higher than reported in [24] for high density L-mode discharges with attached outer divertor. An increase of the emission zone of the injected species was detected and the loss of photons was estimated. However, the D/XB values represent upper limits and further modelling is required.

Qualitatively similar results with stronger reduction of intrinsic light in divertor detachment were obtained in DIII-D under comparable plasma conditions [19]. Methane injection with the PPI provides $\left[\frac{D}{XB}\right]^{CH_4 \rightarrow CH}_{\mathrm{A}\ ^2\Delta \rightarrow \mathrm{X}\ ^2\Pi}$ of about 98+/-25, normalised to the full emission range, and thus about 2.5 larger in comparison to a typical attached case. Both experiments indicate that indeed the reduction of ϕ^{CD}_{A-X} (fig.7) and $\phi^{C_2}_{d-a}$ is accompanied by a reduction of the eroded hydrocarbon particle flux when the plasma detaches. The question, whether the flux reduction is linked to a reduction of Y^{chem}_C, is topic of a forthcoming paper.

5. Summary and conclusion

Passive emission spectroscopy was applied to determine effective inverse photon efficiencies, hydrocarbon fluxes and erosion yields in different fusion devices. This was achieved by means of in-situ calibration with hydrocarbon injection - either with a single inlet or with systems distributed on the circumference. Effective inverse photon efficiencies for a variety of hydrocarbons, specifically in the case of the CH Gerö band and of the C_2 Swan band, were measured in reference experiments in TEXTOR without surface contamination. The normalised photon-per-particle production efficiencies for $\eta(CII) \simeq 0.5$, $\eta(CI) \simeq 0.2$ and $\eta(H_\gamma) \simeq 0.2$ as well as the observation of CH^+ during methane injection in TEXTOR indicate that at high electron temperatures the break-up chain, though a multi-step process, goes substantially via molecular ions. The TEXTOR benchmark experiment verified the current database for the methane break-up, used in different erosion/deposition models. An independent verification of the database was done at DIII-D [16].

A comparison of D/XB values for methane, obtained in different machines as a function of T_e, was presented and compared to calculations with HYDKIN. The re-erosion of higher hydrocarbons built up during injection of methane was observed and its influence on the effective inverse photon efficiencies for methane discussed.

At JET, the part of the erosion yield associated with the production of C_2H_y was measured in the outer divertor in L-mode: it was as low as 0.6%. Improvements in the data analysis for chemical erosion yields were brought forth by TEXTOR. Higher hydrocarbons play a minor role. Physical and chemical erosion are balanced and each process lay about 3.0% at the temperature maximum for chemical - hence total - erosion.

First results on hydrocarbon injections into the detached outer divertor of DIII-D and ASDEX Upgrade were shown, indicating a drastic reduction of the hydrocarbon flux by more than one order of magnitude during detachment, although higher effective inverse photon efficiencies were measured than predicted by HYDKIN. This regime has been identified as favourable for ITER and further experiments on different machines are foreseen to exploit its advantage of low chemical erosion.

This work was done in the frame of the European Task Force on Plasma-Wall Interaction.

References

[1] R. Pitts et al., Plasma Phys. Control. Fusion **47** (2005) B303

[2] V. Philipps et al., Plasma Phys. Control. Fusion **45** (2003) A17

[3] A. Kirschner et al., Nucl. Fusion **40** (2000) 989

[4] J. Roth et al., Nucl. Fusion **44** (2004) L21

[5] A. Pospieszczyk et al., J. Nucl. Mater. **145-147** (1987) 547

[6] http://adas.phys.strath.ac.uk

[7] S. Brezinsek et al., Plasma Phys. Control. Fusion **47** (2005) 615

[8] R. Janev and D. Reiter, Phys. Plasmas **9** (2002) 4071

[9] A. Pospieszczyk et al., UCLA, Report PPG-125 (1989)

[10] S. Brezinsek et al., Physica Scripta **T111** (2004) 42

[11] U. Fantz et al., J. Nucl. Mater. **337-339** (2005) 1087

[12] T. Nakano et al., Nucl. Fusion **42** (2002) 689

[13] R.C. Isler et al., Phys. Plasmas **8** (2001) 4470

[14] M.F. Stamp et al., Physica Scripta **T91** (2001) 13

[15] P.T. Greenland and S. Brezinsek, FZJ - ISSN 0944-2952, Report Juel-4156 (2004)

[16] P. Stangeby et al., this conference

[17] M. Groth et al., this conference

[18] R. Pugno et al., J. Nucl. Mater. **337-339** (2005) 985

[19] A. McLean et al., this conference

[20] Y. Xu et al., this conference

[21] O. Schmitz et al., this conference

[22] http://www.eirene.de/eigen

[23] A. Huber et al., Physica Scripta **T111** (2004) 101

[24] R. Pugno et al., 30th EPS Contr. Fus. and Plasma Phys., St. Petersburg (2003)

[25] S. Brezinsek et al., 32th EPS Plasma Phys., Tarragona (2005)

[26] P. Coad et al., this conference

[27] A. Pospieszczyk et al., J. Nucl. Mater. **241-243** (1997) 821

[28] D.G. Whyte et al., Nucl. Fusion **41** (2001) 1243

Tables

Table 1

species	$CH(CD)$ Gerö band		C_2 Swan band	
	$\frac{D}{XB}$ EXP	$\frac{D}{XB}$ JR	$\frac{D}{XB}$ EXP	$\frac{D}{XB}$ JR
CH_4	27	37	1030	-
C_2H_4	35	53	40	25
C_2H_6	30	46	59	28
C_3H_8	19	28	41	20
CD_4	36	(46)	930	-
C_2D_4	31	(65)	48	(33)
C_2D_6	27	(57)	65	(37)

Table 2

experiment	species	span [nm]	$\left[\frac{D}{XB}\right]^{\textbf{span}}_{\text{A }^2\Delta\rightarrow\text{X }^2\Pi}$	$f(T_{rot}, \lambda_{span})$	$\left[\frac{D}{XB}\right]^{\textbf{full range}}_{\text{A }^2\Delta\rightarrow\text{X }^2\Pi}$
ASDEX Upgrade [11]	CH	430.0-431.5	154	2.8	55
ASDEX Upgrade [23]	CH	430.0-431.5	11-56	2.8	4-20
DIII-D [17]	CH	427.0-431.5	71	1.8	39
JET [10]	CD	429.4-430.9	154-168	2.8	55-60
JET [22]	CD	427.8-431.5	100	1.9	53
JET [14]	CD	427.8-431.5	80	1.9	42
TEXTOR [23]	CH	430.0-431.5	100-240	2.8	32-110
TEXTOR [here]	CD	429.5-431.0	101	2.8	36
TEXTOR [here]	CH	430.0-431.5	76	2.8	27

Table captions

Table 1: Break-up of different types of C_xH_y in D plasmas ($T_e = 35eV$) and C_xD_y in H plasmas ($T_e = 45eV$). Effective D/XB values are related to the full emission range. Values in brackets are calculated under the assumption of ordinary hydrocarbon injection. Table 2: D/XB value normalisation: $f(T_{rot}, \lambda_{span})$ values for the Gerö band in different experiments with CD_4 or CH_4 injection (at different T_e values).

Figure captions

Figure 1: a) Measured and modelled spectra of the A-X band of CD^+ and CD. b) No difference in the ro-vibrational population of the C_2 Swan band for similar plasmas.

Figure 2: CD_4 injection in TEXTOR: a) 2D pattern of CD light, b) Penetration depth for C_2, CII, CD and D_γ, and c) ERO modelling of the CD light pattern.

Figure 3: Normalised $\left[\frac{D}{XB}\right]^{CH_4 \rightarrow CH}_{\mathrm{A}\ ^2\Delta \rightarrow \mathrm{X}\ ^2\Pi}$ observed in different fusion devices and calculated values from HYDKIN as function of T_e.

Figure 4: Observation of ϕ_{C_2} during CH_4 injection in ASDEX Upgrade.

Figure 5: In-situ determination of Y_C^{chem} attributed to C_2H_y in JET.

Figure 6: Determination of Y_C^{chem} and Y_C^{phys} by simultaneous observation of CH, CII and D_γ in TEXTOR.

Figure 7: Gerö band in the outer divertor of ASDEX Upgrade under attached and detached (w/wo methane injection) plasma conditions.

Figures

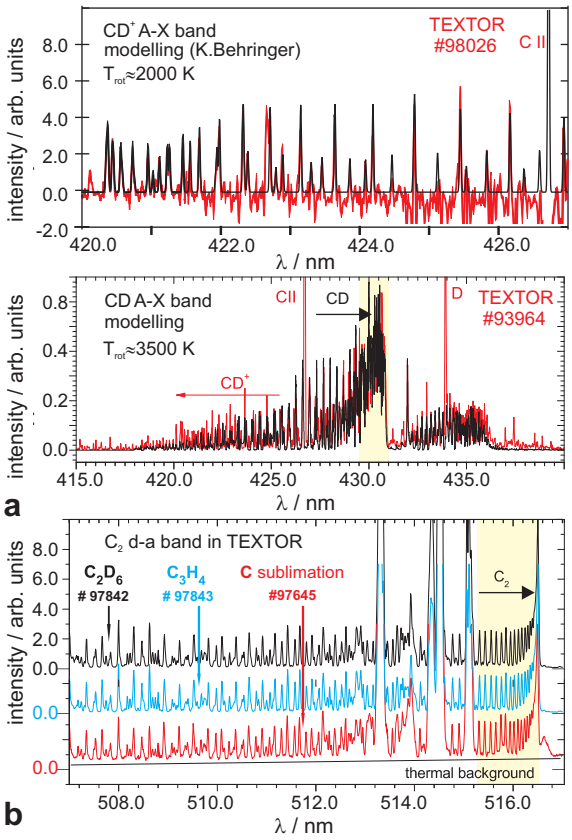

Figure 1:

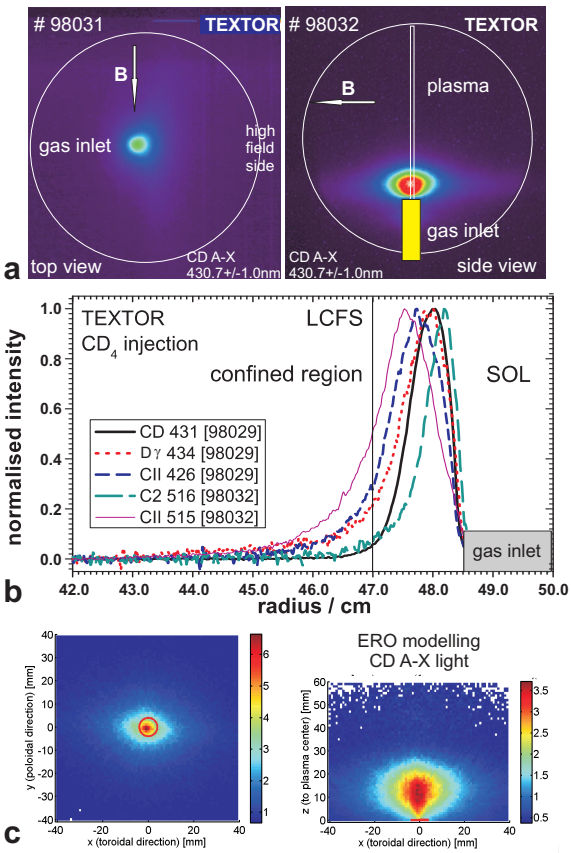
98031
TEXTOR
B
gas inlet
high field side
top view
CD A-X 430.7+/-1.0nm
98032
TEXTOR
B
plasma
gas inlet
CD A-X 430.7+/-1.0nm
side view
a
TEXTOR
CD4 injection
LCFS
confined region
SOL
CD 431 [98029]
Dγ 434 [98029]
CII 426 [98029]
C2 516 [98032]
CII 515 [98032]
gas inlet
normalised intensity
radius / cm
b
ERO modelling
CD A-X light
y (poloidal direction) [mm]
x (toroidal direction) [mm]
z (to plasma center) [mm]
x (toroidal direction) [mm]
c

Figure 2:

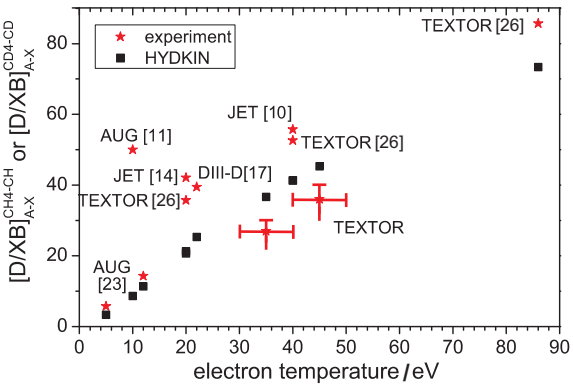
experiment
HYDKIN
TEXTOR [26]
JET [10]
AUG [11]
TEXTOR [26]
JET [14]
DIII-D[17]
TEXTOR [26]
TEXTOR
AUG
[23]
[D/XB]CH4-CH A-X or [D/XB]CD4-CD A-X
electron temperature / eV
0
10
20
30
40
50
60
70
80
90
0
20
40
60
80

Figure 3:

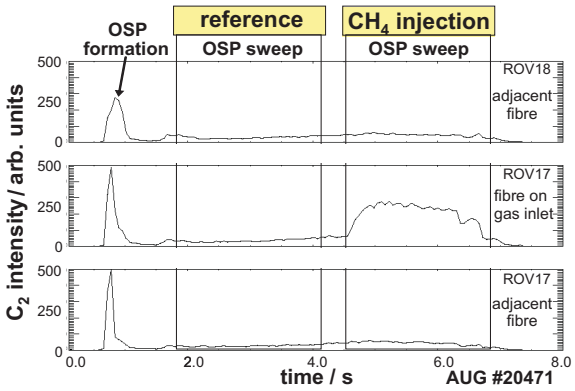
reference
CH4 injection
OSP formation
OSP sweep
OSP sweep
ROV18
adjacent fibre
ROV17
fibre on gas inlet
ROV17
adjacent fibre
C2 intensity / arb. units
500
250
0
0.0
2.0
4.0
6.0
8.0
time / s
AUG #20471

Figure 4:

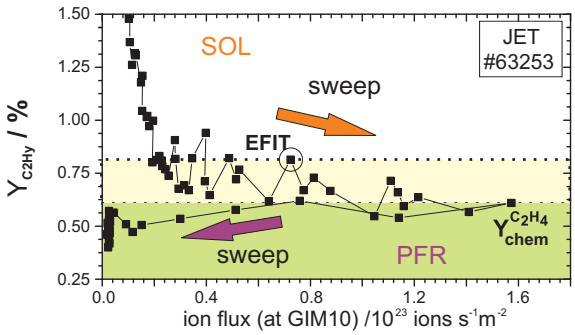
1.50
1.25
1.00
0.75
0.50
0.25
Y_{C2Hy} / %
SOL
JET
#63253
sweep
EFIT
sweep
PFR
$Y^{C_2H_4}_{chem}$
0.0
0.4
0.8
1.2
1.6
ion flux (at GIM10) /10^{23} ions $s^{-1}m^{-2}$

Figure 5:

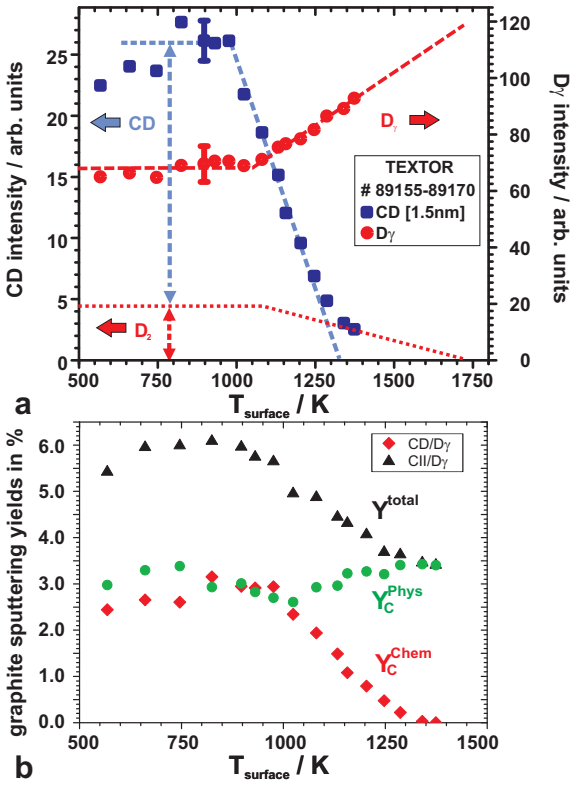
CD intensity / arb. units
Dγ intensity / arb. units
CD
D1
D2
TEXTOR
89155-89170
CD [1.5nm]
Dγ
T surface / K
a
graphite sputtering yields in %
CD/Dγ
CII/Dγ
Y total
Y Phys C
Y Chem C
T surface / K
b

Figure 6:

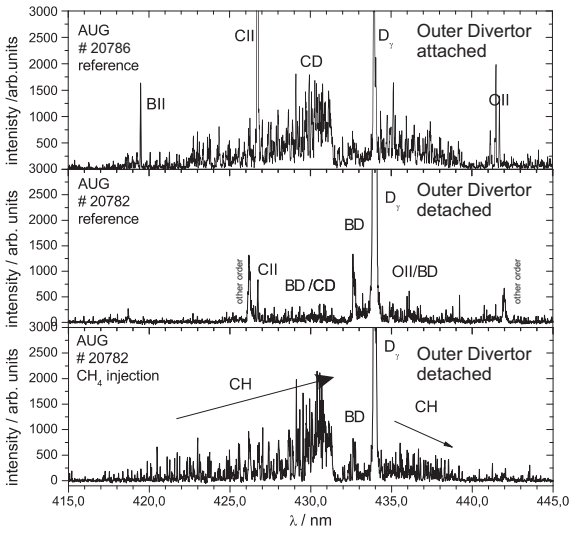
AUG
20786
reference
BII
CII
CD
D_γ
Outer Divertor
attached
CII
intenisty /arb.units
AUG
20782
reference
D_γ
Outer Divertor
detached
BD
other order
CII
BD /CD
OII/BD
other order
intensity / arb. units
AUG
20782
CH_4 injection
D_γ
Outer Divertor
detached
CH
BD
CH
intensity / arb. units
λ / nm

Figure 7: